

## Green synthesis of iron nanoparticles using *Pistacia-atlantica* leaf extract for enhanced removal of Cr(VI) from aqueous solution



Sahar Hasanzadeh<sup>a</sup>, Sobhan Mortazavi-Derazkola<sup>b</sup>, Rasoul Khosravi<sup>c,\*</sup>

<sup>a</sup> Student Research Committee, Birjand University of Medical Sciences, Birjand, Iran

<sup>b</sup> Medical Toxicology and Drug Abuse Research Center (MTDRC), Birjand University of Medical Sciences, Birjand, Iran

<sup>c</sup> Department of Environmental Health Engineering, School of Health, Birjand University of Medical Sciences, Birjand, Iran

### ARTICLE INFO

#### Keywords:

Cr (VI)  
Adsorption  
Kinetic study  
Fe nanoparticles

### ABSTRACT

The discharge of chromium-containing wastewater from various industries into aqueous environments is regarded as an important and challengeable matter due to its high toxicity. The application of conventional methods for eliminating this pollutant are often very expensive and difficult. Therefore, the adsorption process has been introduced as a desirable and effective method for removing chromium ions from aqueous media. In this research, iron nanoparticles (Fe-NPs) were synthesized using *Pistacia-atlantica* leaf extract as a reducing agent, then they were characterized by DLS, XRD, FT-IR, FESEM/EDS, and TEM techniques and its effectiveness to eliminate hexavalent chromium (Cr (VI)) from aqueous solutions was carried out. The capability of the batch adsorption procedure was assessed under different operational factors, such as initial pH, adsorbent dose and initial Cr (VI) concentration. Optimum adsorption conditions were determined at initial pH of 2, Cr (VI) concentration of 25 mg L<sup>-1</sup> and adsorbent dose of 0.24 g L<sup>-1</sup>. Based on the obtained results, the highest removal efficiency (99.9%) by the adsorption process was occurred at pH of 2, concentration of 5 mg L<sup>-1</sup> and 30 min of operational time. On the other hand, the results showed that the percentage of the pollutant elevated by increasing the contact time and amount of adsorbent dose, whereas that of was declined by increasing the initial concentration of Cr (VI). Besides, the experimental equilibrium data was evaluated by Langmuir, Freundlich, and Temkin isotherm models, and the outcomes revealed conformity with the Langmuir isotherm model. The Cr (VI) adsorption utilizing Fe-NPs adhered to a pseudo-first-order kinetic model. Eventually, thermodynamic studies demonstrated that the adsorption of Cr (VI) onto the surface of the Fe-NPs is endothermic and spontaneous.

### 1. Introduction

Heavy metals, owing to toxicity at low dosages in soil and water and devastating impacts on water environments, have become a notable global concern for general health of human beings and living organisms [1,2]. In recent years, the widespread use of toxic chromium (Cr) compounds in various industries, such as textile, tanning, metal mining and smelting, metal plating, pulp production and wood preservatives, has led to the release of significant quantities of this pollutant into water environments [3,4]. Among different states of Cr, hexavalent chromium (Cr (VI)) has been considered as a highly toxic, non-biodegradable, and carcinogenic substance due to the formation of several health problems for human beings, including skin irritation, acute pulmonary edema, liver disease (damage), and lung cancer [5,6]. Regarding the United States Environmental Protection Agency (USEPA), the highest permissible value of limit of Cr (VI) ions in drinking water is

determined as 0.05 mg L<sup>-1</sup> [7]. Furthermore, according to the USEPA report, Cr (VI) is classified as one of the 25 hazardous and dangerous substances for living creatures [8]. Additionally, the World Health Organization (WHO) has proposed that the maximum level of total Cr in drinking water is considered as 50 µg L<sup>-1</sup> [5]. Therefore, due to the highly toxic and harmful nature of Cr (VI), it is necessary to remove it from the environment [9]. Various methods have been currently deployed to eliminate heavy metals, especially Cr (VI), from water and wastewater, such as ion exchange, membrane filtration, coagulation, biological treatment, electrochemical precipitation, photocatalytic reduction, solvent extraction and reverse osmosis [10–12]. Most of these methods are ineffective for the eradication of heavy metals owing to low efficiency, remarkable economic costs, sludge disposal and restrictions in engineering applications [13,14]. In this sense, surface adsorption has received much attention compared to other approaches for removing metal ions from water sources due to its cost-effectiveness,

\* Corresponding author.

E-mail addresses: [shr5431@gmail.com](mailto:shr5431@gmail.com) (S. Hasanzadeh), [S.mortazavi23@yahoo.com](mailto:S.mortazavi23@yahoo.com) (S. Mortazavi-Derazkola), [khosravi.r89@gmail.com](mailto:khosravi.r89@gmail.com) (R. Khosravi).

easy operation, high elimination efficiency, low energy consumption, and compatibility with the environment [5,9]. Unfortunately, studies have shown that among various types of adsorbents, activated carbon, silicone, and polymer resin, are not cost-effective at high dosage [15,16]. On the other hand, nowadays, the application of nanostructured adsorbents have been developed for decontaminating a wide variety of contaminants (e.g., heavy metals, organic pollutants, mineral anions, and bacteria) because of characteristics like their small size, high adsorption capacity, and strong reactivity [17]. Therefore, they can be considered as a good substitute for other adsorbents in water remediation from contaminants [18]. In addition, in extensive studies, the utilization of single and multi-walled carbon nanotubes have been developed to degrade heavy metals [19,20]. Since there are various substances for removing heavy metals from aqueous environments, nanoscale zero-valent iron has been considered as an effective reducing agent for removing Cr (VI) from aqueous solutions given its low cost, high active surface, and high adsorption capacity. In general, iron nanoparticles (Fe-NPs) are widely used to remove heavy metals, due to some characteristics such as small diameter of particles, large surface area, reactivity, and very high reduction potential [21]. Furthermore, in recent years, extensive attention has been paid to the green synthesis of Fe-NPs using plant extracts compared to other traditional and common methods as it is a simple, non-toxic, sustainable and cost-effective method with the high potential of recovery and reuse. Besides, it does not demand of harsh circumstances such as high pressure, energy, and temperature or the utilization of toxic chemical compounds [22]. The synthesis of nanoparticles by chemical and physical methods, despite the production of pure nanoparticles with suitable characteristics, is not cost-effective and it requires complex and special equipment [23]. In the green synthesis process, biological compounds present in plant extracts, including polyphenols, act as reducing and stabilizing agents in the synthesis process of nanoparticles [24]. These factors affect the size and morphology of nanoparticles. The green synthesis of Fe-NPs using different plant extracts has been reported by many researchers. For example, Hoag et al. [25] synthesized ZVI utilizing a green tea (*Camellia sinensis*) extract containing a range of polyphenols. Wang [26] constructed stable iron-polyphenol complex nanoparticles (Fe-P NPs) using a leaf extract of eucalyptus. FeO/Fe<sub>3</sub>O<sub>4</sub> nanoparticles were successfully synthesized using a pomegranate (*Punica granatum*) leaf extract in the study by Rao et al. [27]. *Pistacia-atlantica* is a plant that has a high antioxidant and antimicrobial activity and is highly useful for the green synthesis of nanomaterials [28].

So far, there is a lack of works focusing on utilizing the green synthesis of Fe-NPs using *Pistacia-atlantica* leaf extract for removing toxic metal ions. Thus, the aim of the present study is to employ the green fabrication of Fe-NPs using *Pistacia-atlantica* leaf extract for the elimination of Cr (VI) from aqueous media.

## 2. Materials and methods

### 2.1. Reagents and chemicals

All chemicals used in this study, such as Iron (III) sulfate (Fe (SO<sub>4</sub>)<sub>3</sub>·7 H<sub>2</sub>O), Potassium dichromate (K<sub>2</sub>Cr<sub>2</sub>O<sub>7</sub>), 1,5-diphenylcarbazide (DPC), Acetone (CH<sub>3</sub>COCH<sub>3</sub>), Nitric acid (65%) and Methanol (CH<sub>4</sub>O) were purchased from Merck, and all these materials were of high purity. In the current work, *Pistacia-atlantica* extract was used for the green synthesis process, and deionized water was also used to provide the desired solutions. During the adsorption process experiments, the pH medium was adjusted with hydrochloric acid and sodium hydroxide (1 N).

### 2.2. Preparation of stock solution

A stock solution of 1000 mg·L<sup>-1</sup> of Cr(VI) was prepared by dissolving 2.82 g of potassium dichromate (K<sub>2</sub>Cr<sub>2</sub>O<sub>7</sub>) in 1 L of deionized

water, and whole working solutions were provided through diluting the prepared stock solutions with deionized water [29].

### 2.3. Extract preparation

*Pistacia-atlantica* leaves were collected from the eastern regions of Iran and were washed several times with distilled water to remove the dust on the leaves. Then, they were placed to dry in an oven at a temperature of 60 °C for 48 h, and finally, the resulting substances were completely powdered using a grinder. 12 g of the prepared powders was transferred to the decanter funnel and its surface was covered with methanol, and a stirrer was used to completely mix the ingredients. After approximately 72 h, the desired plant was formed. Finally, they were separated from methanol by a rotary device and placed in a refrigerator at 4 °C for further use [30,31].

### 2.4. Green synthesis of Fe-NPs

Trivalent iron sulfate (Fe (SO<sub>4</sub>)<sub>3</sub>) was used as a precursor for the synthesis of Fe-NPs. 50 mL of extracted *Pistacia-atlantica* leaves was added drop by drop to 50 mL of the solution (Fe<sub>2</sub>(SO<sub>4</sub>)<sub>3</sub>) with a ratio of 1:4 at room temperature in the presence of nitrogen. Next, NaOH (2 N) was added until the pH of the solution reached about 12. The resulting mixture was stirred using a magnetic stirrer for 1 h. The formation of Fe-NPs was indicated by the appearance of a black precipitate in the mixture. In the next step, the nanoparticles were separated using a centrifuge at a speed of 6000 rpm for 5 min, and then, they were washed with distilled water around three times continuously. Finally, the Fe nanoparticles were dried in an oven at 60 °C for roughly 48 h and stored in a closed container for further utilization [32,33].

### 2.5. Characterization

Fe nanoparticles synthesized by the green method were subjected to various characterization techniques, including Fourier transform infrared spectroscopy (FTIR) (spectrum two, Perkin Elmer, US), FESEM (ZEISS Company, Sigma VP model, Germany) equipped with EDX detectors (Oxford Instruments, England), transmission electron microscopy (TEM) (EM10C-100KV device, Zeiss, Germany), X-ray spectroscopy (XRD) (Philips Pw 1830 Netherlands), dynamic light scattering and zeta potential (Nano Brook-90plus, Brookhaven, US) and vibrating sample magnetometer (VSM, model LBKFB, Meghnatis Daghigh Kovir Company).

### 2.6. Batch reactor experiments

The uptake experiments of Cr (VI) utilizing Fe NPs were carried out discontinuously. The influence of multiple parameters, such as pH (2–9), Cr (VI) dosage (5–10 mg L<sup>-1</sup>), Fe NPs content (0.05–0.5 g L<sup>-1</sup>) and contact time (5–180 min), was surveyed on the adsorption of Cr (VI). After experiments, the Fe NPs were eliminated from the solution, and the remaining content of Cr (VI) in the suspension was quantified.

The uptake capacity of the Fe-NPs was computed based on the following equation:

$$q_e = \frac{(C_0 - C_e) \times V}{m} \quad (1)$$

Where  $C_0$  (mg L<sup>-1</sup>) and  $C_e$  (mg L<sup>-1</sup>) are the initial concentration and equilibrium concentration of Cr (VI), respectively.  $M$  (g) is the mass of Fe-NPs, and  $V$  (L) is the solution volume. Furthermore, the removal efficiency of Cr(VI) was calculated using relation 2:

$$R (\%) = (C_0 - C_e) / C_0 \times 100\% \quad (2)$$

## 2.7. Determination of zero-point charge

The point of  $pH_{zpc}$  of Fe-NPs was determined as follows: a solution containing 0.01 M NaCl was prepared. Then, the value pH of the solution was adjusted in the range of 2–12 using 0.1 M NaOH and 0.1 M HCl solutions. After that, 0.01 g of nanoparticles was added to the solution and stirred for 24 h. After the desired time, the final pH ( $pH_{final}$ ) was measured using a pH meter. The  $pH_{zpc}$  value can be determined from the curve through intersecting the initial pH ( $pH_{initial}$ ) line of the  $pH(\Delta H_{initial} - pH_{final})$  graph versus  $pH_{initial}$  [34].

## 2.8. Thermodynamic study

The thermodynamic study of the adsorption process requires three main parameters, including standard enthalpy ( $\Delta H^\circ$ ), standard free energy ( $\Delta G^\circ$ ), and standard entropy ( $\Delta S^\circ$ ). In this study, to specify the thermodynamic factors of the Cr(VI) adsorption procedure utilizing Fe NPs, multiple tests were carried out. Herein, entropy changes ( $\Delta S^\circ$ ), enthalpy changes ( $\Delta H^\circ$ ), and standard Gibbs free energy changes ( $\Delta G^\circ$ ) were calculated as follows:

$$\ln k_c = -\Delta H^\circ/RT + \Delta S^\circ/R \quad (3)$$

$$\Delta G = -RT \ln k_c = \Delta H - T\Delta S \quad (4)$$

Where R is the universal gas constant (8.314 J mol<sup>-1</sup> K), T is the temperature (K), and  $k_c$  is the distribution coefficient. The Van't Hoff linear plot and the thermodynamic factors specified for Cr (VI) uptake process.

The equilibrium constant value ( $K_c$ ) was calculated by Eq. 5:

$$k_c = q_e/c_e \quad (5)$$

The negative sign of  $\Delta G^\circ$  value indicates the spontaneity (feasibility) of the adsorption process. Moreover, a positive value of  $\Delta H^\circ$  indicates that the adsorption process is naturally endothermic, and the adsorption capacity increases with increasing temperature degree. The positive quantity of  $\Delta S^\circ$  reveals the affinity of the adsorbent to the adsorbed substance in the solution, and some structures change between contaminant molecules and active sites of adsorbents. The positive value of entropy change ( $\Delta S^\circ$ ) demonstrates that the degree of freedom (psychology) enhances at the solid-liquid interface during adsorption process [35].

## 2.9. Adsorption isotherm

Langmuir, Freundlich, and Temkin isotherm models are used to fully reveal interaction between sorbent and sorbate [36]. Additionally, the Langmuir model is adopted to determine the adsorption capacity of the adsorbent. In this model, it is assumed that monolayer adsorption is occurred on the surface of homogeneous adsorbents without specific interactions among the adsorbent molecules. However, in the Freundlich model, multilayer adsorption is occurred on the adsorbent surface containing heterogeneous adsorption sites [37,38]. The Temkin model assumes that the heat level of all the adsorbent molecules decreases linearly with increase in the adsorbent surface coverage due to adsorbent-adsorbate interactions during the adsorption process [39]. Temkin constant,  $b_T$ , is defined as the heat of adsorption variable (J/mol), which determines the endothermic ( $b_T < 1$ ) and exothermic ( $b_T > 1$ ) nature of the adsorption reaction. The linear equations of Freundlich, Langmuir, and Temkin models are expressed below:

$$\log q_e = \log K_F + 1/n \log C_e \quad (6)$$

$$\frac{C_e}{q_e} = \frac{1}{q_{max} K_L} + C_e/q_{max} \quad (7)$$

$$q_e = RT/b_T \ln(K_T C_e) \quad (8)$$

According to Eq. 7,  $q_e$  (mg g<sup>-1</sup>) and  $C_e$  (mg L<sup>-1</sup>) represent the concentration of Cr (VI) adsorbed by Fe-NPs at equilibrium state, and  $q_m$  or (mg g<sup>-1</sup>)  $q_{max}$  is the maximum adsorption capacity of Fe-NPs. In the Langmuir equation through monolayer adsorption,  $K_L$  (L mg<sup>-1</sup>) is the adsorption equilibrium constant, which is dependent on the heat of adsorption. The constants  $q_{max}$  and  $K_L$  can be obtained from the slope intercept of the plot of  $C_e/q_e$  versus  $C_e$ . Based on Eq. 6,  $n$  and [(mg g<sup>-1</sup>) (L mg<sup>-1</sup>)<sup>1/n</sup>]  $K_F$  are constants of the Freundlich model, which are reliant on the adsorption intensity and adsorption capacity, respectively. The values of  $K_F$  and  $1/n$  can be calculated from the slope of the linear graph between  $\log C_e$  and  $\log q_e$ .

## 2.10. Adsorption kinetics

Several kinetic models including pseudo-first-order and pseudo-second-order can be employed to describe the kinetic behavior of the adsorption process. The adsorption rate can be described using pseudo-first-order model and is expressed as the following linear equation:

$$\ln(q_e - q_t) = \ln q_e - \frac{K_1 t}{2.303} \quad (9)$$

Here,  $q_e$  and  $q_t$  (mg g<sup>-1</sup>) represent the adsorption quantity of Cr (VI) from aqueous solutions at equilibrium and time  $t$  (min), and  $k_1$  (1/min) is the first-order equilibrium rate constant.

The linear equation of the pseudo-second-order kinetic model is usually described as follows:

$$\frac{t}{q_t} = \frac{1}{K_2 q_e^2} + \frac{t}{q_e} \quad (10)$$

In this equation,  $q_e$  and  $q_t$  are the adsorption capacity of Cr (VI) ions at equilibrium and desired time (mg g<sup>-1</sup>), respectively, and  $k_2$  (g. (mg min)<sup>-1</sup>) reflects the constant value of the adsorption rate.

## 2.11. Reusability study

The fabrication of adsorbents with a high ability of reusability in constructive adsorption-desorption runs is regarded as one of the notable factors in declining operational expenses of the uptake process [40–42]. Herein, the adsorption-desorption process of Cr(VI) ions was examined for a maximum of five runs employing Fe-NPs. To this end, under optimized circumstances, 0.1 g of Fe-NPs was mixed with an aqueous solution including Cr(VI) (5 mg L<sup>-1</sup>) at 25 °C. After adsorption, the Fe-NPs were under centrifugation at 6000 rpm. At the end of the time, the Fe-NPs were separated from aqueous media, and the Cr(VI) content isolated from the adsorbents was quantified.

## 3. Results and discussion

### 3.1. Characterization of the adsorbents

#### 3.1.1. FESEM Analysis

FESEM analysis was conducted to evaluate the morphological attributes of the Fe-NPs before and after the Cr (VI) adsorption. As displayed, before Cr (VI) adsorption, the sample of Fe-NPs exhibits a rough surface with different sizes of pores, and the pores is filled with Cr (VI), after the surface adsorption. Therefore, due to filling the pores and increasing the size of the particles, it can be concluded that Fe-NPs could successfully adsorb Cr (VI) [43].

#### 3.1.2. EDX analyses

EDX technique was used to investigate the elemental composition of Fe-NPs synthesized with *Pistacia-atlantica* extract (Fe-NPs @PAE). The results of elemental analysis of Fe-NPs before and after adsorption of Cr (VI) are displayed in Fig. 2. As the findings exhibit, Fe (60.2%), O (39.2% W) and S (0.5% W) are present in the structure of the synthesized Fe-NPs, demonstrating the successful formation of the Fe-NPs. The

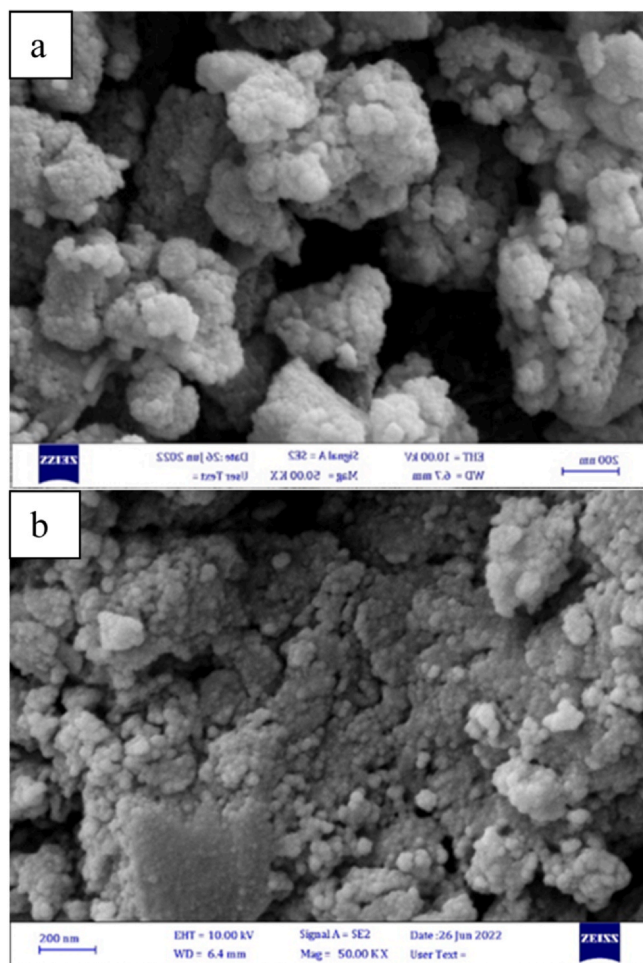


Fig. 1. FESEM images of Fe-NPs before and after reaction with chromium.

peaks of C and O can be attributed to the carbonyl groups of polyphenolic compounds in *Pistacia-atlantica* leaf extract, which acts as a covering and reducing agent and greatly helps to stabilize the green Fe-NPs [44,45]. The presence of element S before and after Cr adsorption can be owing to the presence of the sulfate group of the precursor ( $\text{FeSO}_4^3$ ). The presence of Cr in the elemental composition of synthesis nanoparticles indicated that the Cr (VI) ions were adsorbed on the surface of the Fe-NPs [46].

### 3.1.3. TEM analysis

Structural shape and size of biosynthesized Fe-NPs were determined by the TEM analysis, the corresponding results are displayed in Fig. 3. Accordingly, it can be seen that the structure of the synthesized adsorbent has a spherical with oval shape and the adhesion and connection of particles in different parts, which can be due to the extracts placed on the structure. The average diameter of the particles was in the range of 30–50 nm.

### 3.1.4. FTIR analysis

FTIR analysis was performed to characterize structural changes in the Fe-NPs nanoparticles pre- and post- Cr (VI) elimination. In the FT-IR spectrum of *Pistacia-atlantica* leaf extract (Fig. 4, a), the wavelength of  $3421\text{cm}^{-1}$  is related to the functional group of hydroxyl polyphenols (OH) [47,48]. This group is responsible for the reduction of  $\text{Fe}^{2+}$  to  $\text{Fe}^0$  [43]. As can be seen, the peaks related to the extract have appeared in the Fe-NPs spectrum (Fig. 4,b), demonstrating that the desired extract was effective on the nanoparticle. However, the peak intensity at  $3421\text{cm}^{-1}$  decreased significantly after the synthesis of Fe-NPs,

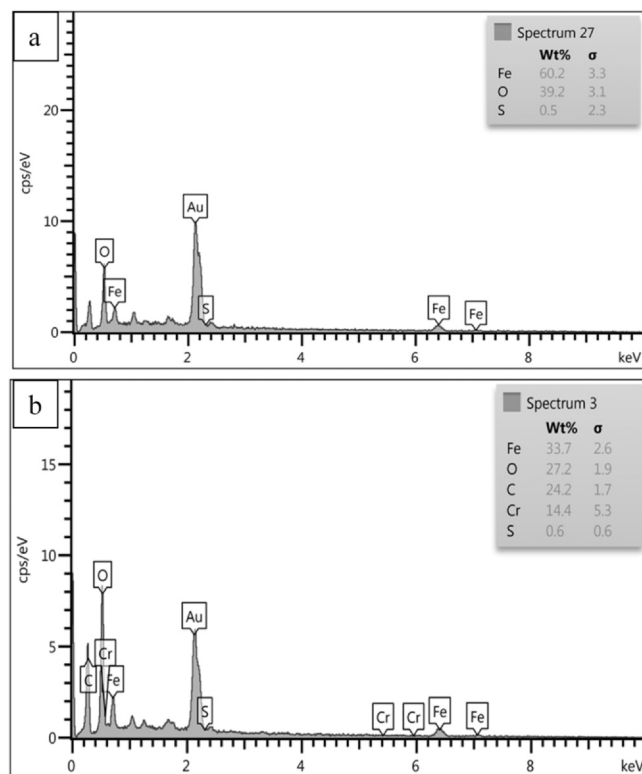


Fig. 2. EDS spectrum for the Fe-NPs before (a) and after reaction with Cr (VI) (b).

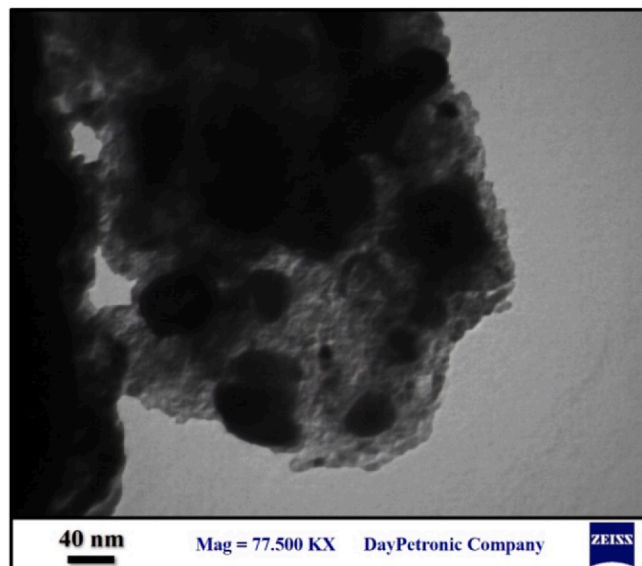


Fig. 3. TEM image of Fe-NPs.

indicating that the polyphenols in the extract are involved in the production of Fe-NPs. The bands observed at  $2922$  and  $2851\text{cm}^{-1}$  are related to C-H stretching vibrations of aliphatic hydrocarbons with  $-\text{CH}_2$  and  $\text{CH}_3$  functional groups [43], [49]. The peaks at  $1609\text{cm}^{-1}$  and  $1445\text{cm}^{-1}$  indicated the stretching vibrations of C=C double bond in the aromatic rings of the phenolic compounds (e.g., flavonoids, polyphenols) present in the extracts, which are unsaturated hydrocarbon compounds [23]. The peaks at  $1316$ ,  $1032\text{cm}^{-1}$  may be assigned to C-O and C=O stretching vibrations [50]. According to the FTIR spectrum of Fe-NPs, the peak at  $546\text{cm}^{-1}$  corresponded to the stretching vibrations of Fe-O in  $\text{Fe}_3\text{O}_4$  [36,51].

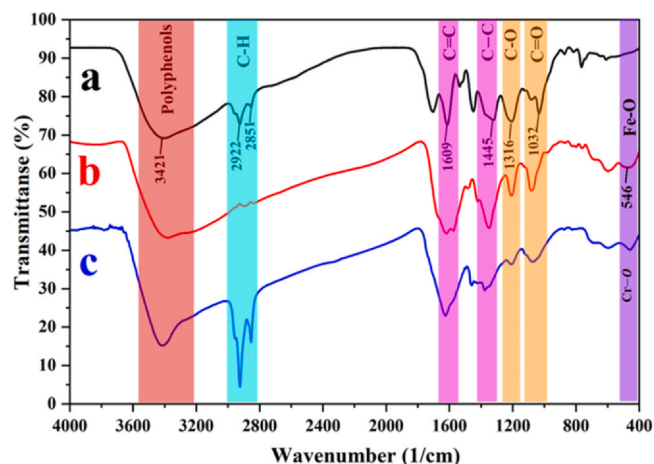


Fig. 4. FTIR spectra of (a) *Pistacia-atlantica* extract, (b) synthesized iron nanoparticles before reaction with Cr (VI) and (c) after adsorption of Cr (VI).

### 3.1.5. XRD Analysis

XRD patterns of Fe-NPs before and after Cr (VI) adsorption are depicted in Fig. 5. A broad peak, around  $2\theta$  of  $20\text{--}30^\circ$ , can be observed. The patterns have a lack of distinct diffraction peaks, demonstrating that Fe-NPs are amorphous. The broaden peaks at  $20\text{--}30^\circ$  could be attributed to the adsorption of organic materials from extracts, which act as capping/stabilizing agents. Similar results were observed in other studies [22,23,36].

### 3.1.6. VSM analysis

The magnetic behavior of the biosynthesized Fe-NPs in the magnetic field in the range of  $0 \leq H \leq 20000$  was examined by the VSM analysis at room temperature. As displayed in Fig. 6, the magnetic saturation value of the synthesized nanoparticles ( $M_s$ ) was  $3.16 \text{ emu g}^{-1}$ , revealing that they have magnetic property. Besides, no magnetic hysteresis loop was observed, and the magnetic coercive force ( $H_c$ ) and residual magnetization ( $M_r$ ) were achieved as zero. Therefore, it can be concluded that the Fe-NPs are paramagnetic. The results of this study were in agreement with the research work by [52].

### 3.1.7. DLS analysis

Particle size distribution and zeta potential of Fe-NPs with the intervention of *Pistacia-atlantica* extract were analyzed through the DLS

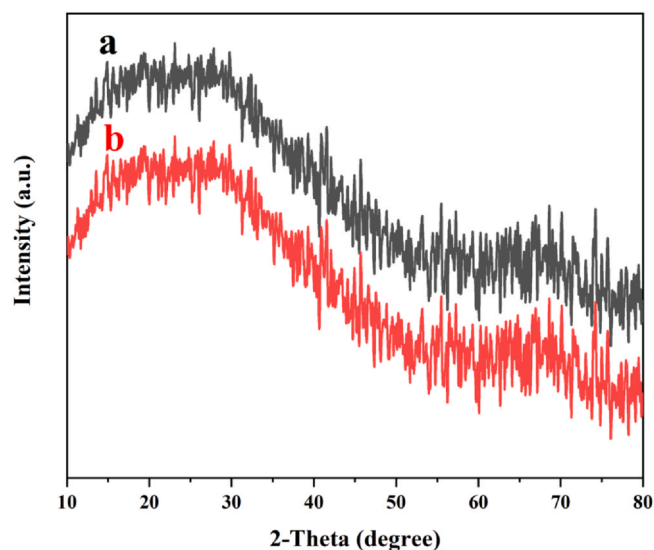


Fig. 5. XRD analysis of synthesized Fe-NPs (a) before and (b) after Cr (VI) adsorption.

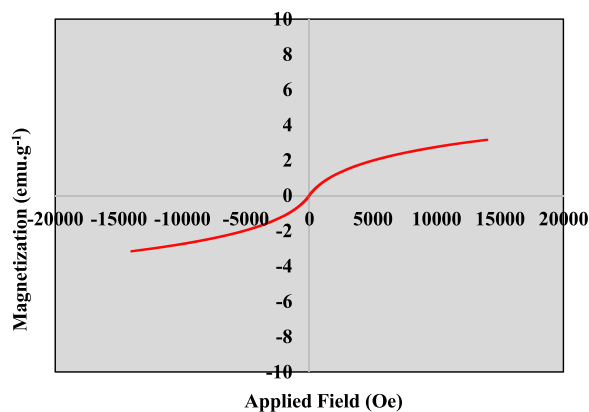


Fig. 6. Magnetic hysteresis curve of Fe-NPs.

analysis. The average hydrodynamic diameter of Fe-NPs was recorded at approximately 800 nm. The size distribution of the synthesized Fe-NPs by the DLS analysis is presented in Fig. 7. As displayed, it can be understood that the tendency to accumulation in the fabricated nanoparticles can be ascribed to their high hydrodynamic diameter [49].

### 3.1.8. Determination of zeta potential

Zeta potential, the charge potential of the double layer around the particles, determines the stability or instability of adsorbents. A high zeta potential of an adsorbent means that it is very stable [34]. Nonetheless, if the zeta potential values are greater than  $+30 \text{ mV}$  or less than  $-30 \text{ mV}$ , disclosing that the adsorbent is considered stable, while the zeta potential approaches zero, it is regarded unstable [50]. Regarding the acquired outcomes, the zeta potential of the Fe-NPs was  $0.31 \text{ mV}$  (Fig. 7, b), which reveals that the Fe-NPs were unstable.

## 3.2. Batch adsorption studies

### 3.2.1. Effect of initial pH

Fig. 8 shows the effect of pH on the removal efficiency of Cr (VI) by Fe-NPs. As displayed in Fig. 8, increasing pH levels from 2 to 9, the Cr (VI) removal efficiency showed a significant decline from 87.71% to 5.86%. The reduction in the removal rate can be linked to the generation of different forms of Cr (VI), including  $\text{Cr}_2\text{O}_7^{2-}$ ,  $\text{CrO}_4^{2-}$ ,  $\text{HCrO}_4^-$ , and  $\text{H}_2\text{CrO}_4$ . Cr (VI) exists in the form of oxy-anionic hydrogen chromate ( $\text{HCrO}_4^-$ ) and dichromate ( $\text{Cr}_2\text{O}_7^{2-}$ ) at pH value range of 2–6, while, in the pH span of above 6 and less than 1, it is in the form of chromate ( $\text{CrO}_4^{2-}$ ) and  $\text{H}_2\text{CrO}_4$  as the main and dominant form of Cr, respectively [49]. In acidic environments, especially pH less than 6.4,  $\text{HCrO}_4^-$  is the dominant form of Cr (VI), which is obtained from the hydrolysis of dichromate. An increase in pH values leads to the formation of  $\text{Cr}_2\text{O}_7^{2-}$  from  $\text{HCrO}_4^-$ . Furthermore, at pH less than 6,  $\text{Fe}^0$  particles can be easily oxidized by Cr (VI) to  $\text{Fe}^{+2}$ , thereby increasing the adsorption of Cr (VI) [43,48]. Therefore, it is drawn that the reduction process (i.e. reduction of Cr (VI) to Cr (III)) under acidic conditions increases the removal efficiency of Cr (VI) [43,53,54]. Furthermore, Cr (VI) surface adsorption studies have demonstrated that the removal efficiency decreases significantly as the pH value of the solution enhances. The reason for increasing removal efficiency at pH of 5 is that, under less acidic media,  $\text{Cr}^{3+}$  ions become dominant rather than protons ( $\text{H}^+$ ) and attracted toward the anionic surface of Fe-NPs; therefore, elimination rate will boost. However, at pH greater than 6, the surface of Fe-NPs becomes more anionic, which will strongly hinder the  $\text{HCrO}_4^-$ ,  $\text{CrO}_4^{2-}$  and  $\text{Cr}_2\text{O}_7^{2-}$  ions. Therefore, these nanoparticles will show minimum results for chromium removal [55]. The point of zero charge can be attributed to the determination of the pH value, which has a zero of the net surface charge. In the pH spans higher than  $\text{pH}_{\text{zpc}}$ , the net surface charge is negative, while the net surface charge is positive in low pHs media. In other words, the adsorbent surface has a

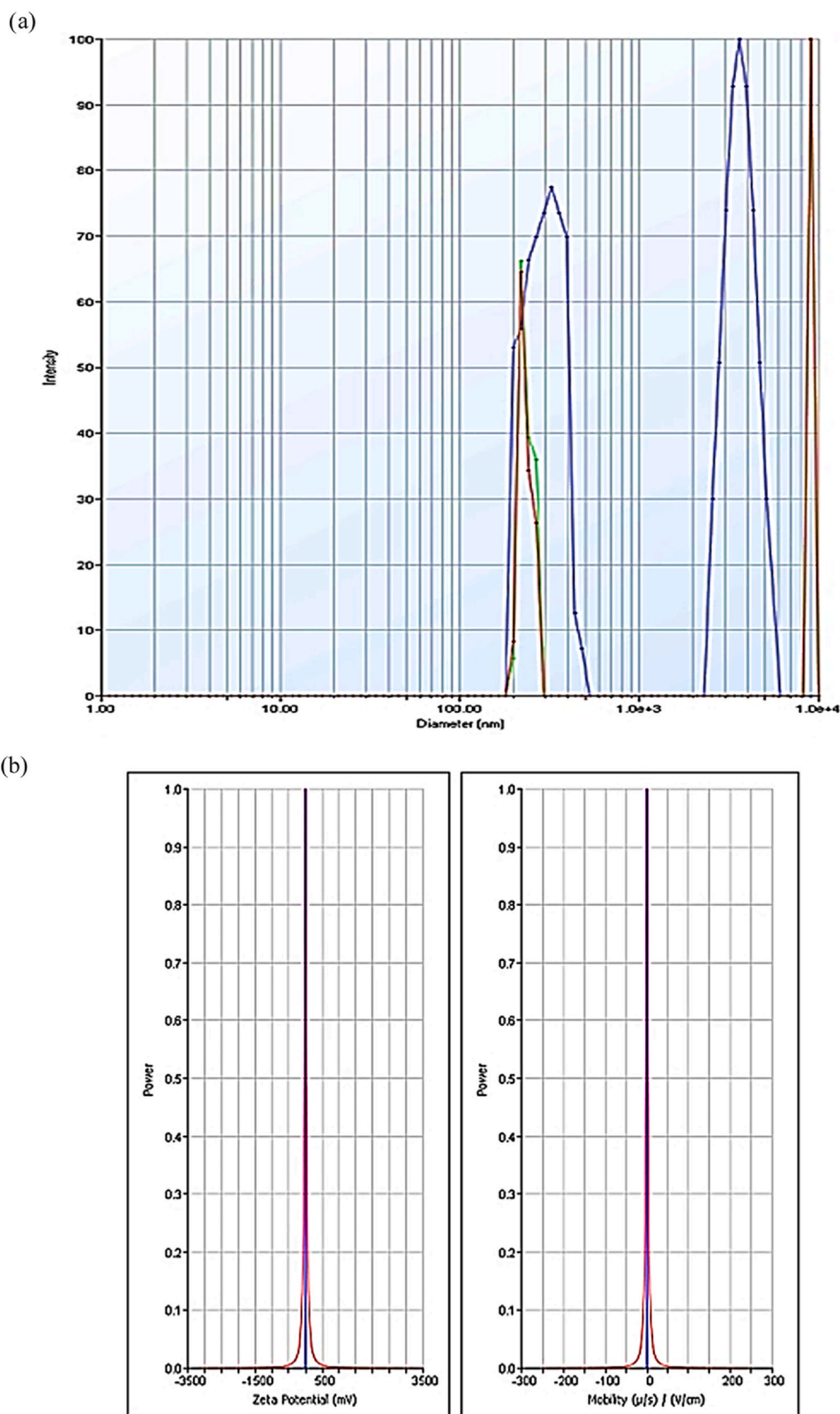
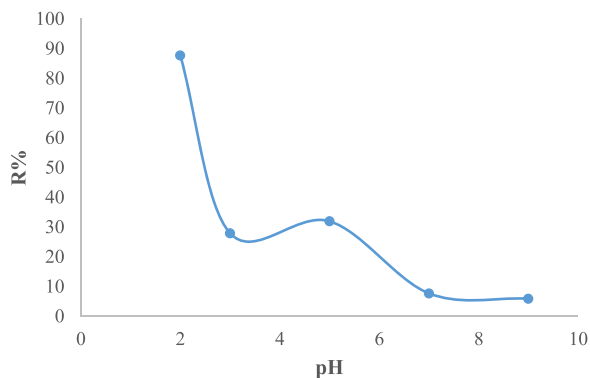


Fig. 7. a) Size analysis of Fe nanoparticles by DLS (b) Zeta potential graph of Fe-NPs.

positive charge at pH values lower than the isoelectric point of the adsorbent and the adsorption capacity is improved due to the strong electrostatic attraction between the adsorbent surface with a positive charge and  $\text{HCrO}_4^-$  ion with a negative charge. On the contrary, at pH values higher than the isoelectric point of the adsorbent, the number of active sites with a negative charge is elevated, whereas that of with a

positive charge is decreased. Consequently, the removal performance of the Cr (VI) utilizing the Fe-NPs decreased because of the electrostatic repulsion between the adsorbent surface and  $\text{HCrO}_4^-$  ions [49,56]. According to the acquired data, the optimized pH level for eliminating the Cr (VI) from aqueous media using the Fe-NPs was determined as 7.12.



**Fig. 8.** Effect of pH on percent removal of Cr (VI) under optimal circumstances (Cr (VI) = 25 mg L<sup>-1</sup>, Time = 30 min, dose = 0.24 g L<sup>-1</sup> NPs, speed = 250 rpm, temperature = 25 °C).

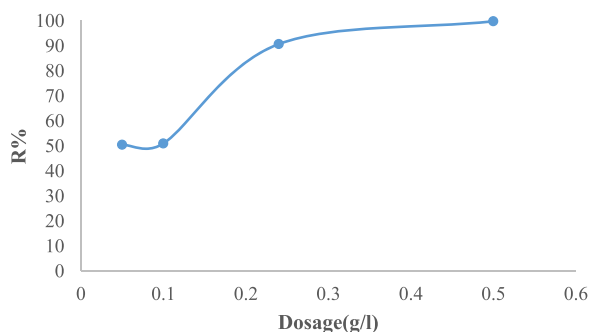


**Fig. 9.** The effect of Fe-NPs dose on the adsorption of Cr (VI) (Cr (VI) = 25 mg L<sup>-1</sup>, Time = 30 min, speed = 250 rpm, temperature = 25 °C).

### 3.2.2. Effect of adsorbent dose

The effect of adsorbent dose on the adsorbent capacity and removal efficiency of Cr (VI) under optimal conditions (Cr(VI) concentration = 25 mg L<sup>-1</sup>, pH = 2, operational time = 30 min) is displayed in Fig. 9. As the outcomes show, with the growing adsorbent concentration from 0.05 to 0.5 g L<sup>-1</sup>, the removal performance enhanced from 50.52% to 99.82%. Additionally, the adsorption efficiency of Cr (VI) reached the highest value (99.82%) under reaction time of 30 min and the adsorbent dose of 0.5 g L<sup>-1</sup>. Elevating in the adsorption efficiency can be attributed to the increase in the availability of active sites on the surface of the adsorbent, which can lead to the further adsorption of Cr (VI) ions. According to the results of the study [57], the improvement of the dosage of different adsorbents, the removal of Cr (VI) grew, which is similar to the increasing trend of the Cr (VI) adsorption efficiency of the present study.

### 3.2.3. Effect of initial concentration of chromium

The effect of initial concentration of Cr (VI) (5–50 mg L<sup>-1</sup>) on its removal efficiency by Fe-NPs was studied (Fig. 10). At the concentrations of 5, 10, and 25 mg L<sup>-1</sup>, the removal proportion of Cr (VI) was obtained as 99.7%, 99.52%, and 88.4%, respectively. Nonetheless, the elimination rate of Cr (VI) decreased significantly to 69.95% at the Cr (VI) concentration of 50 mg L<sup>-1</sup>. It can be concluded that the active sites of Fe-NPs were gradually occupied by Cr (VI) and eventually reduced the removal proportion of Cr (VI) with the enhancement of the Cr (VI) concentration. The outcomes are consistent with the results reported by [56,58].

### 3.2.4. Effect of contact time

Fig. 11 displays the impact of contact time on the Cr (VI) removal. The removal efficiency gradually elevated from 80.8% to 90% as the contact time elevated from 5 to 30 min. Other studies [34,59,60] also reported that the elimination rate of Cr (VI) grew with elevation in the contact time.

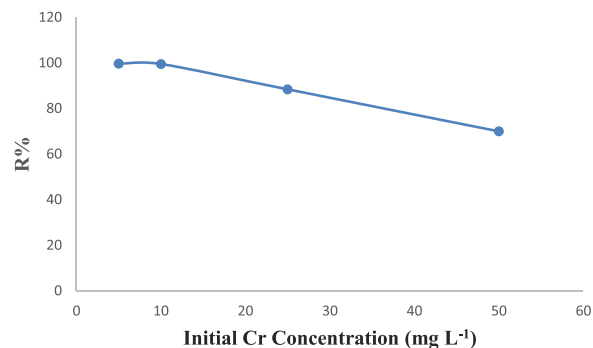


**Fig. 10.** The effect of the initial concentration of chromium on the adsorption performance of Fe-NPs (temperature = 25 °C, initial pH = 2, adsorbent concentration = 0.24 g L<sup>-1</sup>, and contact time = 30 min).

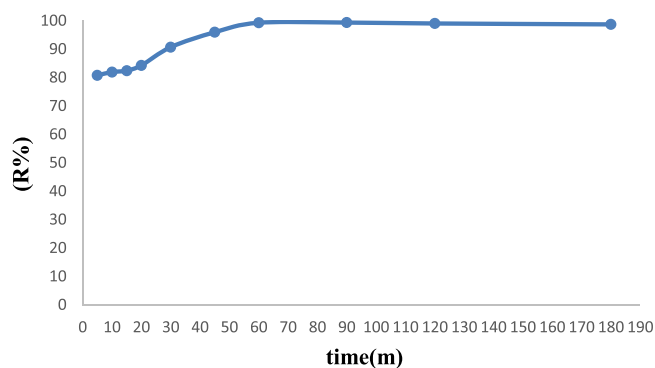


**Fig. 11.** The effect of contact time on the removal efficiency of Fe-NPs (temperature = 25 °C, initial pH = 2, adsorbent concentration = 0.24 g L<sup>-1</sup>, chromium concentration = 25 mg L<sup>-1</sup>).

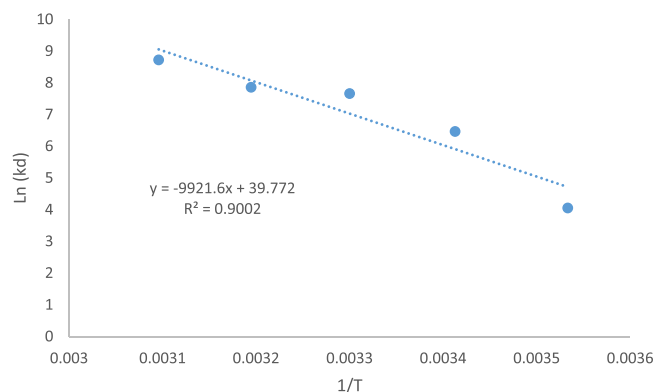


**Fig. 12.** Van't Hoff curve for Cr (VI) adsorption on Fe-NPs.

**Table 1**

Thermodynamic parameters for Cr (VI) removal by Fe- NPs.

T (K)	$\Delta H^\circ$ (Kk. Jmol <sup>-1</sup> )	$\Delta S^\circ$ (Jk <sup>-1</sup> mol <sup>-1</sup> )	$\Delta G^\circ$ (k. Jmol <sup>-1</sup> )
283	82.48	330.6	-9.54
293			-15.76
303			-19.30
313			-20.45
323			-23.43

### 3.3. Thermodynamic studies

Cr (VI) adsorption curve and thermodynamic parameters are represented in Fig. 12 and Table 1, respectively. According to the table, the value of  $\Delta H^\circ$  is 82.48. The positive value of  $\Delta H$  indicates that the endothermic nature of the process. Additionally, the negative value of

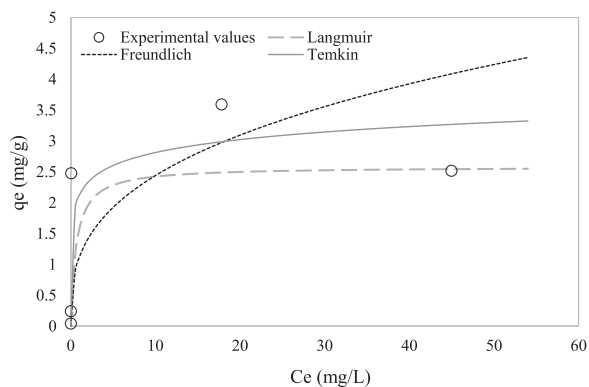


Fig. 13. Plots for the non-linear Langmuir, Freundlich and Temkin isotherm.

$\Delta G^\circ$  indicated that the Cr(VI) adsorption process is spontaneous. The positive value of entropy change ( $\Delta S^\circ$ ) demonstrated that the degree of freedom increases at the solid-liquid interface during uptake process. The obtained findings of the present study are well-fitted with similar published works [61] concerning Cr(VI) adsorption.

### 3.4. Adsorption isotherm

The adsorption isotherms were employed to scrutinize the interaction between Cr (VI) ions and the surface of adsorbents, and also calculate the performance of the adsorbents to eliminate Cr (VI) pollutant from aqueous solutions. The Langmuir, Freundlich, and Temkin isotherm models were utilized. Nonlinear regression and also acquired variables are presented in Fig. 13 and Table 2. According to the obtained findings, it is clear that the Langmuir isotherm model (a correlation coefficient ( $R^2$ ) of 98%) has strong performance to illustrate the adsorption equilibrium manner rather than other models. Furthermore, the results of previously published studies [62,63] are well-fitted with the outcomes of the present work as the adsorption process of Cr (VI) ions followed the Langmuir model. The maximum adsorption capacity ( $q_{max}$ ) based on the Langmuir isotherm method, and also the regression coefficient for the Langmuir, Freundlich, and Temkin models was calculated as 0.98, 0.53, and 0.63, respectively. In the Freundlich isotherm, the parameter of  $n$  indicates the proper process of adsorption which was 2.9 for the Cr (VI) ions. The value of  $n > 1$  indicates that there is a physical interaction between sorbent and adsorbate. It also indicates when  $0 < 1/n < 1$ , a favorable adsorption process occurs. In the Temkin isotherm,  $b_T$  between 8 and 16  $\text{kJ}\cdot\text{mol}^{-1}$ , the adsorption process comes up chemisorption. Since this value is about 8  $\text{kJ}/\text{mol}$ , it is a chemical adsorption process.

Table 2  
Parameters of Langmuir, Freundlich, and Temkin isotherm models.

Isotherm model	Parameters
Langmuir	$q_m = 2.585 \text{ mgg}^{-1}$ $k_l = 1.639 \text{ L}\cdot\text{mg}^{-1}$ $R^2 = 0.98$ RMSE = 1.151 % $\Delta q_e = 65$
Freundlich	$k_F = 1.094 \text{ mgg}^{-1}$ $n = 2.946$ $R^2 = 0.53$ RMSE = 1.192 $\Delta q_e = 238.448\%$
Temkin	$AT (\text{L}/\text{g}) = 1060.4 \text{ L g}^{-1}$ $b_T = 8176 \text{ J mol}^{-1}$ $B = 0.303 \text{ J mol}^{-1}$ $R^2 = 0.63$ RMSE = 0.837 $\Delta q_e = 850.6$

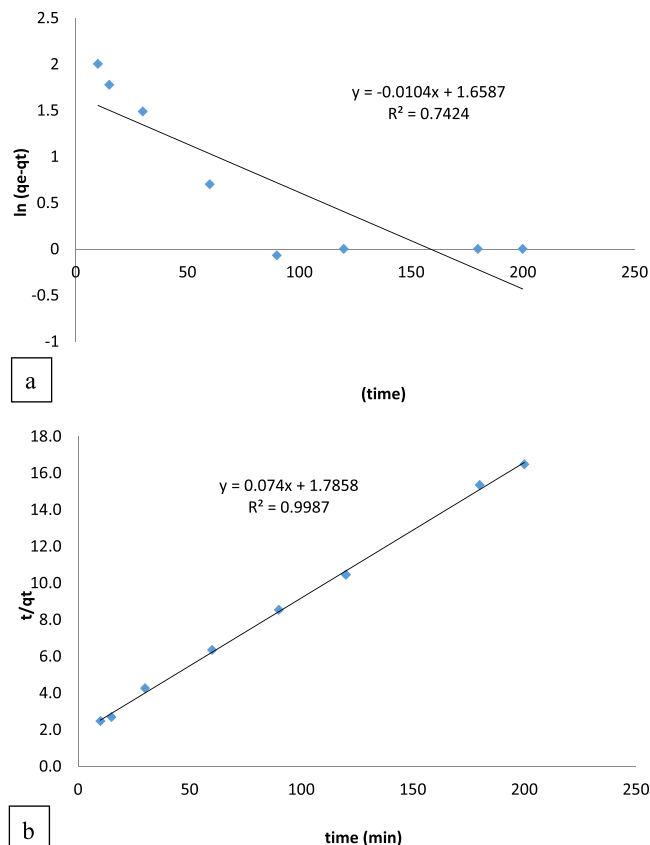


Fig. 14. Pseudo-first-order (a) and pseudo-second-order (b) kinetic models of Cr (VI) adsorption using Fe NPs.

### 3.5. Adsorption kinetics

To determine the adsorption kinetics of Cr (VI) on Fe-NPs and the equilibrium time of the reaction, the removal efficiency was evaluated at contact times (5–180 min) under initial Cr (VI) concentration of  $25 \text{ mg L}^{-1}$  and pH level of 2. The quantified kinetic constants and parameters are presented in Fig. 14 and Table 3. The correlation coefficients acquired for kinetic model revealed that the pseudo-second-order model can be well-fitted for describing the process kinetic manner. Besides, the results demonstrated that the computational adsorption capacity for pseudo-first order and pseudo-second order kinetic models was 8.37 and 67.11, respectively. Moreover, the theoretical  $q_e(\text{cal})$  values were in good agreement with the experimental  $q_e(\text{exp})$  values in terms of pseudo-second-order kinetics. As  $K_2$  coefficient is higher than  $K_1$ , which leads to that the adsorption behavior is well-described by the pseudo-second-order kinetic, suggesting that the rate-limiting step is surface adsorption on the basis of chemisorption mechanism. The adsorption mechanism assumes according to chemisorption, where the adsorbate species interacts with the catalyst surface through chemical bonds. Additionally, it assumes when the rate of site occupation on the catalyst surface is proportional to the square of the number of unoccupied sites, which is a characteristic of specific adsorption processes. In the pseudo-second-order equation, the rate

Table 3  
Parameters of pseudo-first-order Kinetic and Pseudo-second-order Kinetic models.

Pseudo-First-Order Kinetic	$K_1 (\text{min}^{-1})$	$q_e$	$R^2$
	0.017	8.37	0.74
Pseudo-Second-Order Kinetic Model	$K_2 (\text{g}\cdot\text{mg}^{-1}\cdot\text{min}^{-1})$		
	0.004	67.11	0.99

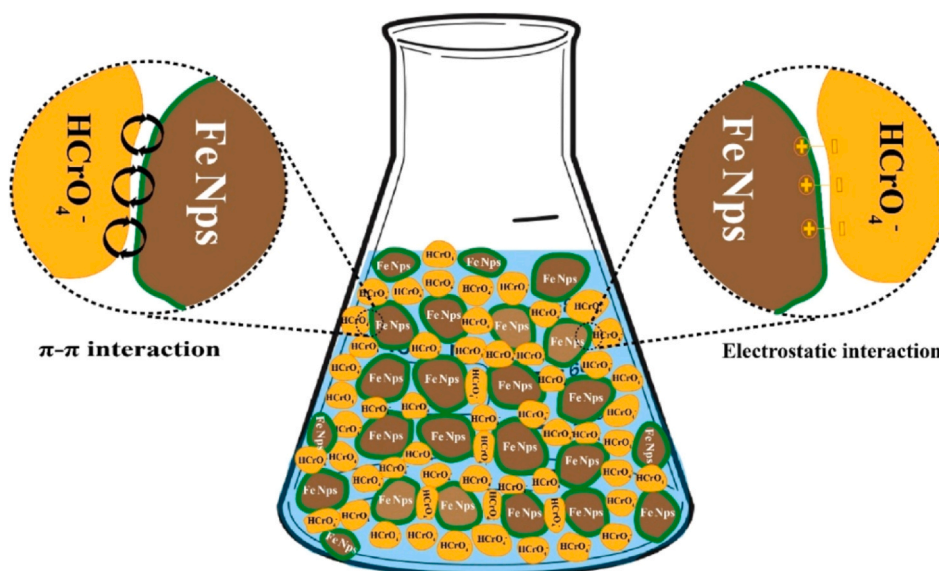


Fig. 15. Illustration of the mechanism.

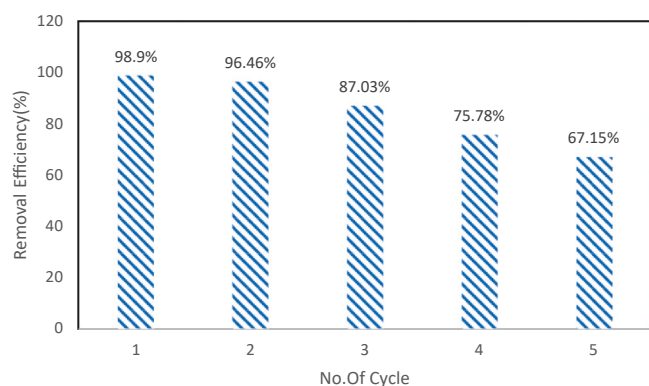


Fig. 16. The adsorption-desorption study for the synthesized Fe-NPs.

constant is usually called  $k_2$ . A high rate constant indicates a faster reaction speed, which means that the reaction proceeds more quickly. The studies [36,49,51] confirmed that the Cr (VI) adsorption process is consistent with the Pseudo-Second-Order Model.

### 3.6. Adsorption mechanism

Considering that the adsorption process follows Langmuir isotherm model, the adsorption of Cr (VI) ions from aqueous media has a single-layer behavior. Regarding the thermodynamic investigation, it was found that adsorption is endothermic, and the adsorption quantity increases with elevating the temperature of the system. Therefore, it can

be concluded that the mechanism of adsorption is chemical, since physical adsorption has an enthalpy value of less than 40 kJ/mol, which means it does not require activation energy, since the physical adsorption process is existence of attractive forces between adsorbent and adsorbate. Chemical adsorption is characterized by having an enthalpy value of more than 40 kJ/mol, because it requires high temperature and activation energy for chemical bonding to take place on the adsorbent surface, and chemical adsorption reactions are irreversible. The pseudo-second-order model is based on the assumption that the rate-limiting step may be a chemical sorption, which involves forces through sharing or exchanging electrons between adsorbent and adsorbate.

### 3.7. Adsorbent recycle

To scrutinize the stability of the investigated material, the adsorption/desorption procedure was examined up to 5 runs (Fig. 16). It is necessary to note that in every stage, the adsorption experiment was conducted under optimized factor circumstances, and the desorption operation was performed for 5 h utilizing a 0.1 M NaOH solution. The outcomes revealed that as the number of recycling adsorbent enhanced, its performance in the elimination of Cr (VI) diminished. The rate of the process was up to 67.15% during 5 successive desorption cycles, which demonstrates the proper performance of the Fe-NPs in the adsorption of Cr (VI) ions from aqueous media. Declining the rate by elevating the number of steps might be linked to the damage and saturation of active sites of the adsorbent. It is also worth noting that a slight difference in the Cr (VI) removal efficiency between the first and second cycles due to the mass loss of the adsorbent during the washing step.

Table 4

Comparison of the results of the present study with other studies.

Adsorbent	pH	Dose (g.L <sup>-1</sup> )	Cr (mg L <sup>-1</sup> ) (Concentration)	Time (min)	Efficiency %	Reference
Iron Nanoparticles-Calcium Alginate Hydrogel Membrane	5.41	12	1	10	99.5	[37]
Ps/nZVI	3	0.5	25	30	90.3	[38]
Granular and powdered Peganum harmala (GPH/PPH)	1.5	10	100	30	100	[54]
Nano zero-Valent iron/Cu	5	0.4	5	60	94.7	[52]
Green Synthesized Iron Nanoparticles	4	1.4	10	10	99.9	[55]
Nanoscale Zero-valent iron (TP-nZVI-OB)	2	1	50	720	99.9	[41]
Green Synthesized Iron Nanoparticles	2	0.24	25	30	99.82	Present study

#### 4. Conclusions

In this study, Fe NPs were biosynthesized using *Pistacia-atlantica* leaf extract as a reducing agent, and they were employed for the elimination of Cr (VI) under laboratory conditions. The results of characterization techniques showed that Fe NPs has an almost spherical structure with an average particle size of 30–50 nm. Also, VSM analysis showed that the magnetic saturation of nanoparticles is about  $3.16 \text{ emu g}^{-1}$ , demonstrating magnetic properties of the synthesized nanoparticles. Optimum adsorption conditions were determined at initial pH of 2, adsorbent dosage of  $0.24 \text{ g L}^{-1}$ , and concentration of chromium of  $25 \text{ mg L}^{-1}$ . Besides, the isotherm and kinetic assessments have exhibited that the adsorption process follows the Langmuir isotherm model (a correlation coefficient of 0.98%) and the pseudo-second-order kinetic model. Based on calculations of the thermodynamic parameters,  $\Delta H$  and  $\Delta S$  were positive and  $\Delta G$  was negative, which disclosed that the Cr (VI) uptake process by the Fe NPs was spontaneous and endothermic.

#### Declaration of Competing Interest

The authors declare that they have no known competing financial interests or personal relationships that could have appeared to influence the work reported in this paper.

#### References

- Zaynab M, et al. Health and environmental effects of heavy metals. *J King Saud Univ Sci* 2022;vol. 34(1):101653. <https://doi.org/10.1016/j.jksus.2021.101653>.
- Suiyi Z, et al. A novel clinoptilolite route to effectively separate Cu for recycling Ca/Zn/Mn from hazardous smelting waterwork sludge. *J Environ Chem Eng* 2024;vol. 12(2):112024. <https://doi.org/10.1016/j.jece.2024.112024>.
- Sharma P, Singh SP, Parakh SK, Tong YW. Health hazards of hexavalent chromium (Cr (VI)) and its microbial reduction. *Bioengineered* 2022;vol. 13(3):4923–38. <https://doi.org/10.1080/21655979.2022.2037273>.
- Zhu F, Ma S, Liu T, Deng X. Green synthesis of nano zero-valent iron/Cu by green tea to remove hexavalent chromium from groundwater. *J Clean Prod* 2018;vol. 174:184–90. <https://doi.org/10.1016/j.jclepro.2017.10.302>.
- Jiang Y, et al. Polyaniline-based adsorbents for removal of hexavalent chromium from aqueous solution: a mini review. *Environ Sci Pollut Res* 2018;vol. 25(7):6158–74. <https://doi.org/10.1007/s11356-017-1188-3>.
- Farooqi ZH, Akram MW, Begum R, Wu W, Irfan A. Inorganic nanoparticles for reduction of hexavalent chromium: physicochemical aspects. *J Hazard Mater* 2021;vol. 402:123535. <https://doi.org/10.1016/j.jhazmat.2020.123535>.
- Monga A, Fulke AB, Dasgupta D. Recent developments in essentiality of trivalent chromium and toxicity of hexavalent chromium: implications on human health and remediation strategies. *J Hazard Mater Adv* 2022;vol. 7:100113. <https://doi.org/10.1016/j.hazadv.2022.100113>.
- A. Kumari, A. Sinha, D.B. Singh, Iron-Based Modified Nanomaterials for the Efficacious Treatment of Cr(VI) Containing Wastewater: A Review, no. July. 2023. doi: <10.1007/978-981-99-2062-4\_13>.
- Yang C, et al. The preparation of a novel iron/manganese binary oxide for the efficient removal of hexavalent chromium [Cr(vi)] from aqueous solutions. *RSC Adv* 2020;vol. 10(18):10612–23. <https://doi.org/10.1039/C9RA105558A>.
- Nasab EA, et al. Efficient purification of aqueous solutions contaminated with sulfadiazine by coupling electro-Fenton/ultrasound process: optimization, DFT calculation, and innovative study of human health risk assessment. *Environ Sci Pollut Res* 2023;0123456789. <https://doi.org/10.1007/s11356-023-28235-z>.
- Eskandarinezhad S, Reza Khosravi RK, Amarzadeh M, Mondal P, Correa Magalhaes Filho FJ. Application of different nanocatalysts in industrial effluent treatment: a review. *J Compos Compd* 2021;vol. 2(5):43–56. <https://doi.org/10.52547/jcc.3.1.5>.
- Amarzadeh M, et al. Statistical modeling optimization for antibiotics decomposition by ultrasound/electro-Fenton integrated process: non-carcinogenic risk assessment of drinking water. *J Environ Manag* 2022;vol. 324:116333. <https://doi.org/10.1016/j.jenvman.2022.116333>.
- Aigbe UO, Osibote OA. A review of hexavalent chromium removal from aqueous solutions by sorption technique using nanomaterials. *J Environ Chem Eng* 2020;vol. 8(6):104503. <https://doi.org/10.1016/j.jece.2020.104503>.
- Liu W, et al. Treatment of Cr VI -containing Mg(OH) 2 nanowaste. *Angew Chem Int Ed* 2008;vol. 47(30):5619–22. <https://doi.org/10.1002/anie.200800172>.
- Jalili M, et al. Green synthesized guar plant composites for wastewater remediation: a comprehensive review. *Polym Bull* 2024;vol. 81(1):247–73. <https://doi.org/10.1007/s00289-023-04758-w>.
- Al-Musawi TJ, Mazari Moghaddam NS, Rahimi SM, Amarzadeh M, Nasseh N. Efficient photocatalytic degradation of metronidazole in wastewater under simulated sunlight using surfactant- and CuS-activated zeolite nanoparticles. *J Environ Manag* 2022;vol. 319:115697. <https://doi.org/10.1016/j.jenvman.2022.115697>.
- Amarzadeh M, Azqandi M, Nateq K, Ramavandi B, Khan NA, Nasseh N. Heterogeneous fenton-like photocatalytic process towards the eradication of tetracycline under UV irradiation: mechanism elucidation and environmental risk analysis. *Water* 2023;vol. 15(13). <https://doi.org/10.3390/w15132336>.
- Ifjen IH, Ikhuria EU, Maliki M, Otabor GO, Aigbodion AI. *Nanostructured Materials: A Review on Its Application in Water Treatment BT - TMS 2022 151st Annual Meeting & Exhibition Supplemental Proceedings*. Cham: Springer International Publishing; 2022. p. 1172–80.
- Alimohammady M, Jahangiri M, Kiani F, Tahermansouri H. Competent heavy metal adsorption by modified MWCNTs and optimization process by experimental design. *J Environ Eng* 2018;vol. 144(11):1–16. [https://doi.org/10.1061/\(asce\)Jec.1943-7870.0001456](https://doi.org/10.1061/(asce)Jec.1943-7870.0001456).
- Eyni H, Tahermansouri H, Kiani F, Jahangiri M. Kinetics, equilibrium and isotherms of Pb2+ adsorption from aqueous solutions on carbon nanotubes functionalized with 3-amino-5a,10a-dihydroxybenzo[b] indeno [2,1-d]furan-10-one. *N Carbon Mater* 2019;vol. 34(6):512–23. [https://doi.org/10.1016/S1872-5805\(19\)60027-2](https://doi.org/10.1016/S1872-5805(19)60027-2).
- Ahmed A, et al. Efficient photocatalytic degradation of toxic Alizarin yellow R dye from industrial wastewater using biosynthesized Fe nanoparticle and study of factors affecting the degradation rate. *J Photochem Photobiol B* 2020;vol. 202:111682. <https://doi.org/10.1016/j.jphotobiol.2019.111682>.
- Pan Z, Lin Y, Sarkar B, Owens G, Chen Z. Green synthesis of iron nanoparticles using red peanut skin extract: Synthesis mechanism, characterization and effect of conditions on chromium removal. *J Colloid Interface Sci* 2020;vol. 558:106–14. <https://doi.org/10.1016/j.jcis.2019.09.106>.
- Yi Y, Tu G, Tsang PE, Xiao S, Fang Z. Green synthesis of iron-based nanoparticles from extracts of *Nephrolepis auriculata* and applications for Cr(VI) removal. *Mater Lett* 2019;vol. 234:388–91. <https://doi.org/10.1016/j.matlet.2018.09.137>.
- Eslami S, Ebrahimzadeh MA, Biparva P. Green synthesis of safe zero valent iron nanoparticles by *Myrtus communis* leaf extract as an effective agent for reducing excessive iron in iron-overloaded mice, a thalassemia model. *RSC Adv* 2018;vol. 8(46):26144–55. <https://doi.org/10.1039/C8RA04451A>.
- Hoag GE, Collins JB, Holcomb JL, Hoag JR, Nadagouda MN, Varma RS. Degradation of bromothymol blue by 'greener' nano-scale zero-valent iron synthesized using tea polyphenols. *J Mater Chem* 2009;vol. 19(45):8671–7. <https://doi.org/10.1039/B909148C>.
- Wang T, Jin X, Chen Z, Megharaj M, Naidu R. Green synthesis of Fe nanoparticles using eucalyptus leaf extracts for treatment of eutrophic wastewater. *Sci Total Environ* 2014;vol. 466–467:210–3. <https://doi.org/10.1016/j.scitotenv.2013.07.022>.
- Rao A, Bankar A, Kumar AR, Gosavi S, Zinjarde S. Removal of hexavalent chromium ions by *Yarrowia lipolytica* cells modified with phyto-inspired FeO/Fe3O4 nanoparticles. *J Contam Hydrol* 2013;vol. 146:63–73. <https://doi.org/10.1016/j.jconhyd.2012.12.008>.
- Golabiazar R, Othman KI, Khalid KM, Maruf DH, Aulla SM, Yusif PA. Green synthesis, characterization, and investigation antibacterial activity of silver nanoparticles using *pistacia atlantica* leaf extract. *Bionanoscience* 2019;vol. 9(2):323–33. <https://doi.org/10.1007/s12668-019-0606-z>.
- Majidi R, Nouri N, Keramatinia M, davarpanah A, Soroush E, Ramezanzadeh B. ZPC-Zn-Al-LDH surface bilayer; toward designing a durable self-healable nano-structured film with the utmost corrosion resistance. *J Taiwan Inst Chem Eng* 2024;vol. 156:105343. <https://doi.org/10.1016/j.jtice.2024.105343>.
- Ebrahimzadeh MA, Naghizadeh A, Amiri O, Shirzadi-Ahodashi M, Mortazavi-Derazkola S. Green and facile synthesis of Ag nanoparticles using *Crataegus pentagyna* fruit extract (CP-AgNPs) for organic pollution dyes degradation and antibacterial application. *Bioorg Chem* 2020;vol. 94:103425. <https://doi.org/10.1016/j.bioorg.2019.103425>.
- Wang Z, Fernández-Blanco C, Chen J, Veiga MC, Kennes C. Effect of electron acceptors on product selectivity and carbon flux in carbon chain elongation with *Megasphaera hexanoica*. *Sci Total Environ* 2024;vol. 912:169509. <https://doi.org/10.1016/j.scitotenv.2023.169509>.
- Shaker Ardakani L, Alimardani V, Tamaddon AM, Amani AM, Taghizadeh S. Green synthesis of iron-based nanoparticles using *Chlorophytum comosum* leaf extract: methyl orange dye degradation and antimicrobial properties. *Heliyon* 2021;vol. 7(2):e06159. <https://doi.org/10.1016/j.heliyon.2021.e06159>.
- Guo D, Li H, Xu Z, Nie Y. Development of pyrene-based MOFs probe for water content and investigations on their mechanochromism and acidochromism. *J Alloy Compd* 2023;vol. 968:172004. <https://doi.org/10.1016/j.jallcom.2023.172004>.
- Bhan C, Singh J, Sharma YC. Development of adsorbent from *Mentha* plant ash and its application in fluoride adsorption from aqueous solution: a mechanism, isotherm, thermodynamic, and kinetics studies. *Int J Phytoremediat* 2021;vol. 23(11):1113–23. <https://doi.org/10.1080/15226514.2021.1880365>.
- Li H, Wang F, Li J, Deng S, Zhang S. Adsorption of three pesticides on polyethylene microplastics in aqueous solutions: Kinetics, isotherms, thermodynamics, and molecular dynamics simulation. *Chemosphere* 2021;vol. 264:128556. <https://doi.org/10.1016/j.chemosphere.2020.128556>.
- Rong K, Wang J, Zhang Z, Zhang J. Green synthesis of iron nanoparticles using Korla fragrant pear peel extracts for the removal of aqueous Cr(VI). *Ecol Eng* 2020;vol. 149:105793. <https://doi.org/10.1016/j.ecoleng.2020.105793>.
- Kalam S, Abu-Khamsin SA, Kamal MS, Patil S. Surfactant adsorption isotherms: a review. *ACS Omega* 2021;vol. 6(48):32342–8. <https://doi.org/10.1021/acsomega.1c04661>.
- Nasseh N, Barikbin B, Taghavi L, Nasserli MA. Adsorption of metronidazole antibiotic using a new magnetic nanocomposite from simulated wastewater (isotherm, kinetic and thermodynamic studies). *Compos B Eng* 2019;vol. 159:146–56. <https://doi.org/10.1016/j.compositesb.2018.09.034>.
- Al-Hazmi GAA, El-Bindary MA, El-Desouky MG, El-Bindary AA. Efficient adsorptive removal of industrial dye from aqueous solution by synthesized zeolitic imidazolate framework-8 loaded date seed activated carbon and statistical physics modeling.

- Desalin Water Treat 2022;vol. 258:85–103. <https://doi.org/10.5004/dwt.2022.28397>.
- [40] Azqandi M, Shahryari T, Fanaei F, Nasseh N. Green construction of magnetic MnFe<sub>2</sub>O<sub>4</sub>/ZIF-8 nanocomposite utilizing extract of Melissa officinalis plant for the photo-degradation of tetracycline under UV illumination. *Catal Commun* 2023;vol. 185:106798. <https://doi.org/10.1016/j.catcom.2023.106798>.
- [41] Moslehi MH, Zadeh MS, Nateq K, Shahamat YD, Khan NA, Nasseh N. Statistical computational optimization approach for photocatalytic-ozonation decontamination of metronidazole in aqueous media using CuFe<sub>2</sub>O<sub>4</sub>/SiO<sub>2</sub>/ZnO nanocomposite. *Environ Res Feb.* 2024;vol. 242:117747. <https://doi.org/10.1016/j.envres.2023.117747>.
- [42] Wang C, Shi P, Guo C, Guo R, Qiu J. CuCo<sub>2</sub>O<sub>4</sub>/CF cathode with bifunctional and dual reaction centers exhibits high RhB degradation in electro-Fenton systems. *J Electroanal Chem* 2024;vol. 956:118072. <https://doi.org/10.1016/j.jelechem.2024.118072>.
- [43] Fazlzadeh M, Rahmani K, Zarei A, Abdoallahzadeh H, Nasiri F, Khosravi R. A novel green synthesis of zero valent iron nanoparticles (NZVI) using three plant extracts and their efficient application for removal of Cr(VI) from aqueous solutions. *Adv Powder Technol* 2017;vol. 28(1):122–30. <https://doi.org/10.1016/j.apt.2016.09.003>.
- [44] Srečković NZ, et al. Application potential of biogenically synthesized silver nanoparticles using *Lythrum salicaria* L. extracts as pharmaceuticals and catalysts for organic pollutant degradation. *RSC Adv* 2021;vol. 11(56):35585–99. <https://doi.org/10.1039/D1RA05570D>.
- [45] Golrizkhatami F, Taghavi L, Nasseh N, Panahi HA. Synthesis of novel MnFe<sub>2</sub>O<sub>4</sub>/BiOI green nanocomposite and its application to photocatalytic degradation of tetracycline hydrochloride: (LC-MS analyses, mechanism, reusability, kinetic, radical agents, mineralization, process capability, and purification of. *J Photochem Photobiol A Chem* 2023;vol. 444:114989. <https://doi.org/10.1016/j.jphotochem.2023.114989>.
- [46] Samadi Z, Yaghmaeian K, Mortazavi-Derazkola S, Khosravi R, Nabizadeh R, Alimohammadi M. Facile green synthesis of zero-valent iron nanoparticles using barberry leaf extract (GnZVI@BLE) for photocatalytic reduction of hexavalent chromium. *Bioorg Chem* 2021;vol. 114:105051. <https://doi.org/10.1016/j.bioorg.2021.105051>.
- [47] Cheng Y, Dong H, Hao T. CaCO<sub>3</sub> coated nanoscale zero-valent iron (nZVI) for the removal of chromium(VI) in aqueous solution. *Sep Purif Technol* 2021;vol. 257:117967. <https://doi.org/10.1016/j.seppur.2020.117967>.
- [48] Liu H, et al. Plant-mediated biosynthesis of iron nanoparticles-calcium alginate hydrogel membrane and its eminent performance in removal of Cr(VI). *Chem Eng J* 2019;vol. 378:122120. <https://doi.org/10.1016/j.cej.2019.122120>.
- [49] Önal ES, Yatkun T, Aslanov T, Ergüt M, Özer A. Biosynthesis and Characterization of Iron Nanoparticles for Effective Adsorption of Cr(VI). *Int J Chem Eng* 2019;vol. 2019:2716423. <https://doi.org/10.1155/2019/2716423>.
- [50] Wei Y, Fang Z, Zheng L, Tsang EP. Biosynthesized iron nanoparticles in aqueous extracts of *Eichhornia crassipes* and its mechanism in the hexavalent chromium removal. *Appl Surf Sci* 2017;vol. 399:322–9. <https://doi.org/10.1016/j.apsusc.2016.12.090>.
- [51] Zhang Y, Jiao X, Liu N, Lv J, Yang Y. Enhanced removal of aqueous Cr(VI) by a green synthesized nanoscale zero-valent iron supported on oak wood biochar. *Chemosphere* 2020;vol. 245:125542. <https://doi.org/10.1016/j.chemosphere.2019.125542>.
- [52] Zaki SAE-F, Kamal A, Ashmawy NA, Shoeib AA. Nano-metals forming bacteria in Egypt. I. Synthesis, characterization and effect on some phytopathogenic bacteria in vitro. *Sci Rep* 2021;vol. 11(1):12876. <https://doi.org/10.1038/s41598-021-92171-6>.
- [53] Khosravi R, et al. Chromium adsorption from aqueous solution using novel green nanocomposite: Adsorbent characterization, isotherm, kinetic and thermodynamic investigation. *J Mol Liq* 2018;vol. 256:163–74. <https://doi.org/10.1016/j.molliq.2018.02.033>.
- [54] Wang Y, Gong Y, Lin N, Yu L, Du B, Zhang X. Enhanced removal of Cr(VI) from aqueous solution by stabilized nanoscale zero valent iron and copper bimetal intercalated montmorillonite. *J Colloid Interface Sci* 2022;vol. 606:941–52. <https://doi.org/10.1016/j.jcis.2021.08.075>.
- [55] Daneshvar N, Salari D, Aber S. Chromium adsorption and Cr(VI) reduction to trivalent chromium in aqueous solutions by soya cake. *J Hazard Mater* 2002;vol. 94(1):49–61. [https://doi.org/10.1016/S0304-3894\(02\)00054-7](https://doi.org/10.1016/S0304-3894(02)00054-7).
- [56] Qu J, et al. KOH-activated porous biochar with high specific surface area for adsorptive removal of chromium (VI) and naphthalene from water: Affecting factors, mechanisms and reusability exploration. *J Hazard Mater* 2021;vol. 401:123292. <https://doi.org/10.1016/j.jhazmat.2020.123292>.
- [57] Wu J, et al. Preparation of highly dispersive and antioxidative nano zero-valent iron for the removal of hexavalent chromium. *Chemosphere* 2021;vol. 262:127733. <https://doi.org/10.1016/j.chemosphere.2020.127733>.
- [58] Shakya A, Agarwal T. Removal of Cr(VI) from water using pineapple peel derived biochars: Adsorption potential and re-usability assessment. *J Mol Liq* 2019;vol. 293:111497. <https://doi.org/10.1016/j.molliq.2019.111497>.
- [59] Cherdchoo W, Nithetham S, Charoenpanich J. Removal of Cr(VI) from synthetic wastewater by adsorption onto coffee ground and mixed waste tea. *Chemosphere* 2019;vol. 221:758–67. <https://doi.org/10.1016/j.chemosphere.2019.01.100>.
- [60] Samuel MS, Bhattacharya J, Raj S, Santhanam N, Singh H, Pradeep Singh ND. Efficient removal of Chromium(VI) from aqueous solution using chitosan grafted graphene oxide (CS-GO) nanocomposite. *Int J Biol Macromol* 2019;vol. 121:285–92. <https://doi.org/10.1016/j.ijbiomac.2018.09.170>.
- [61] Irshad MA, et al. Enhancing chromium removal and recovery from industrial wastewater using sustainable and efficient nanomaterial: A review. *Ecotoxicol Environ Saf* 2023;vol. 263:115231. <https://doi.org/10.1016/j.ecoenv.2023.115231>.
- [62] Foroutan R, et al. Nickel ions abatement from aqueous solutions and shipbuilding industry wastewater using ZIF-8-chicken beak hydroxyapatite. *J Mol Liq* 2022;vol. 356:119003. <https://doi.org/10.1016/j.molliq.2022.119003>.
- [63] Li S, Wang C, Dong K, Zhang P, Chen X, Li X. MIL-101(Fe)/BiOBr S-scheme photocatalyst for promoting photocatalytic abatement of Cr(VI) and enrofloxacin antibiotic: performance and mechanism. *Chin J Catal* 2023;vol. 51:101–12. [https://doi.org/10.1016/S1872-2067\(23\)64479-1](https://doi.org/10.1016/S1872-2067(23)64479-1).